International Journal of Thermodynamics (IJoT)
ISSN 1301-9724 / e-ISSN 2146-1511
https://dergipark.org.tr/en/pub/ijot

Vol. 27 (No. 3), pp. 006-014, 2024
doi: 10.5541/ijot.1390518
Published online: September 1, 2024

Research Article

Investigation of Photovoltaic Membrane Desalination Utilizing Storage Heat in Solar Cells

[1*] H. A. Abdul Kareem, [1]A. N. Khalifa, [1]A. J. Hamad

[1]Middle Technical University, Engineering Technical College- Baghdad
E-mail: [1]* huseinali1987@gmail.com

Received 15 November 2023, Revised 12 February 2024, Accepted 13 March 2024

Abstract

Solar-assisted Photovoltaic-Membrane Distillation (PMD) is a passive tool to cool and distillate salty water. A theoretical study was conducted in the current work using the COMSOL Multiphysics version 5.6 to develop the CFD model of the PMD. The meteorological data of Baghdad- Iraq was obtained using Meteonorm software V8.0.3.Effects of membrane thickness, space between evaporation and condensation layer, height of fins, number of fins, and inlet water temperature on cell temperature and water productivity were investigated. Thickness of 100 μm exhibited a minimum temperature polarization and maximum membrane coefficient. Space thickness of 2.5 mm exhibited a temperature difference of 4°C between evaporation and condensation layers. Integrating the PMD system into solar panel reduced the cell surface temperature by 7°C. Adding a heat sink of 5 fins with a fin height of 2 cm resulted in a maximum cell temperature of 50 °C and yielded water at point 0.615 kg/h.m^2 rate.

Keywords: *Membrane distillation; CFD simulations; cooling solar PV panels; green technology.*

1. Introduction

The world has turned to search for renewable and clean energy that is environmentally friendly due to the massive consumption of fossil fuels that leads to ozone layer depletion and global warming. Among renewable energies, solar energy, especially PV solar systems, is a promising energy that can subsidize and reduce the consumption of fossil fuels. The conversion of solar energy into power in solar cells is shallow and is about 14 to 18%. The rest of the solar energy is solar radiation that has not been converted into energy which stored in the solar cell as thermal energy and causing a rise in the cell's temperature. The high cell temperature negatively impacts cell performance and reduces the cell's life span. The deviation from the cell's standard operating conditions and the PV panel conversion efficiency are decreased by 0.4 to 0.5% per 1 °C[1].

Rabie et al. 2022[2] introduced the hybridization of high-concentrating photovoltaic (HCPV) with membrane distillation (MD). Numerically, membrane distillation was introduced experimentally. The study aimed to keep the cell's temperature within the standard temperature design. Aleid, 2019 [3] studied effect of membrane thickness on water productivity, three stages of MDS models were investigated. Shi Y et al. 2019 [4] used a photovoltaic-membrane distillation device that can simultaneously produces a clean water and power from the solar energy. Zhao et al. 2020 [5] studied integration of a photovoltaic module (PVM) integrated with a direct contact membrane distillation system (DCMD). The heat generated in the PV panels was used for water pureness. A mathematical model for both DCMD and PVM was proposed, and the numerical results were validated by comparing them with the experiment. Kumar, 2015 [6] proposed a solar distillation system to supply a potable water to urban settlements by combining solar-powered hot water installations with water purification systems. Chiavazzo et al. 2018 [7] proposed a low-cost multistage solar distiller that operates on one sun irradiance. The unit stage was built from three layers; the first and third layers are called hydrophilic, and the second was a hydrophobic microporous membrane. Baloch et al. 2015 [8] Cell surface cooling was experimental and numerical investigated. The simulation model was built using the ANSYS-Fluent software of version 6.3. Popovici et al.2016 [9] introduced a numerical study for reducing the photovoltaic panel's temperature using an air-cooled heat sinks. The heat sink was conceived as a ribbed wall and consisted of a with high thermal conductivity material. Li et al. 2020 [10] developed a novel PV solar-powered stand-alone sweeping gas membrane desalination system. A solar thermal collector was installed for thermal energy collection, and a PV solar array was established to generate AC power. Wang et al. 2020 [11] tested a multistage membrane distillation device (MSMD) and installed it at a back of solar panel. The 5-stage photovoltaics-membrane distillation-evaporative crystallizer (PV-MD-EC) system showed that the productivity of such a system was around 2.45 kg/h.m^2, with a lower solar cell temperature of 48℃.

In the current work, a Photovoltaics-membrane distillation unit (PMD) was modeled and simulated using the COMSOL Multiphysics 5.6 software. Modeling of the PVM unit was applied on July 1st which is considered the hottest day in Baghdad- Iraq (33.3 ° N, 44.14° N, and 34 m elevation) . In the current work, a Photovoltaics-membrane distillation unit (PMD) was modeled and simulated using the

*Corresponding Author

COMSOL Multiphysics 5.6 software. Modeling of PVM unit was applied in 1-July, which is considered the hottest day in Baghdad- Iraq, with a 33.3 ° N, 44.14° N, and 34 m elevation. A passive method was used to cool a PV cell, where a heat generated in the cell and rejected outside using different fluids such as water or air. Issue of storing the heat in the cells was studied. This heat was used for two purposes: cooling the solar panel and desalinating brackish water. Effects of membrane thickness, space between evaporation and condensation layer, height of the fins, number of fins, and inlet water temperature on the cell temperature and water productivity were investigated.

2. Module Description

The PMD system commonly consists of single or multistage. Each stage consists of several layers of hydrophilic membranes working as evaporators or condensers. The principle of any PMD system is to minimize distance between the thin hydrophilic layers; thus, cycle of evaporation and condensation processes was carried out at ambient pressure. Figure 1 shows a single-stage PMD, where the hydrophilic (evaporation layer) adheres directly to the aluminum plate, directly in contact with the back of the solar panel. Water was supplied to the PMD unit by pumping or gravity force; the evaporator layer was wetted by capillary action. The first aluminum plate transfers generated heat in the PV panel to the salty water. In contrast, the last aluminum layer comes into contact with the heat sink to dissipate the accumulated heat in the PV panel as latent heat of evaporation. The salty water comes into contact with the first hot aluminum layer; hence, part of the salty water evaporates and transfers through the steel mesh layer and the membrane, and finally, reaches the condensing layer. In the condenser layer, the vapor condensate to a fresh water and lose the latent heat of evaporation to the aluminum plate in the multistage system or to the heat sink in the single-stage system. For each case, the heat sink was placed at the last cooling stage. Table 1 shows dimensions of the PMD layers. Salinity of salty water was about 400 PPM.

Table 1. Dimensions of the PMD model layers.

Dimension	Value
Solar cell	16×16×0.46 cm
Aluminum sheet (two layers)	16×16×0.07 cm
Hydrophilic layer (evaporation)	16×16×0.1 cm
Steel mesh (two layers)	16×16×0.25 cm
Hydrophobic layer membrane	16×16×0.01 cm
Hydrophilic layer (condensation)	16×16×0.1 cm
Inlet and outlet water tube diameter	0.035 cm
heat sink	5 fins, 2cm high

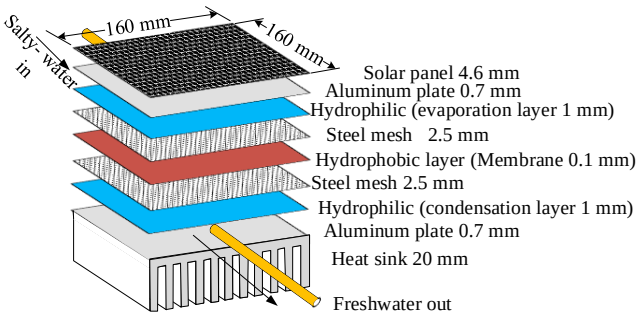

Figure 1. Schematic diagram of PMD system.

3. PMD System Simulation Model

The COMSOL Multiphysics version 5.6 was used to develop the CFD model of the PMD. Meteorological data for Baghdad- Iraq, including global solar radiation and ambient temperature, was obtained from Metronome software V8.0.3. Governing equations, assumptions, and boundary conditions were mentioned in the next section. Three temperature values were calculated for the PMD unit; back cell surface temperature (T_{Cell}), hydrophilic evaporation layer temperature (T_{Evap}) and hydrophilic condensation layer temperature (T_{Cond}), as shown in Figure 2.Two kinds of mesh generators were utilized in implementing the model. The first type was a free normal triangular mesh which was designed for the solar panels, aluminum plates and fins, with a maximum element size of 0.62 m. The second type was free extra fine element-size triangular mesh, which was utilized for domain of laminar flow (evaporation and condensation layers and hydrophobic membrane. The maximum element size for this type was 0.557m, and the number of elements for the PVM model was 712760, as shown in Figure 3. Normally, the residuals for the converged numerical solution are illustrated in Figure 4. Moreover, Figure 5 shows the structure of the COMSOL computation processes.

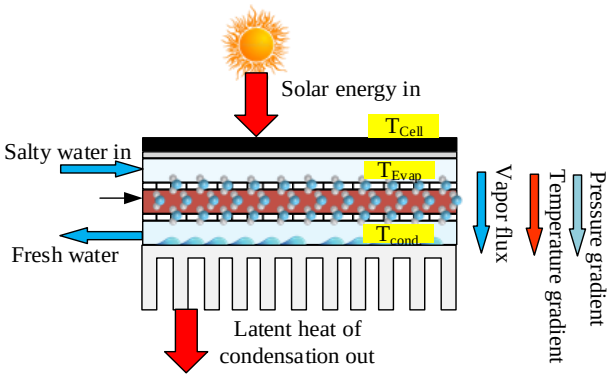

Figure 2. Schematic diagram of the PMD system.

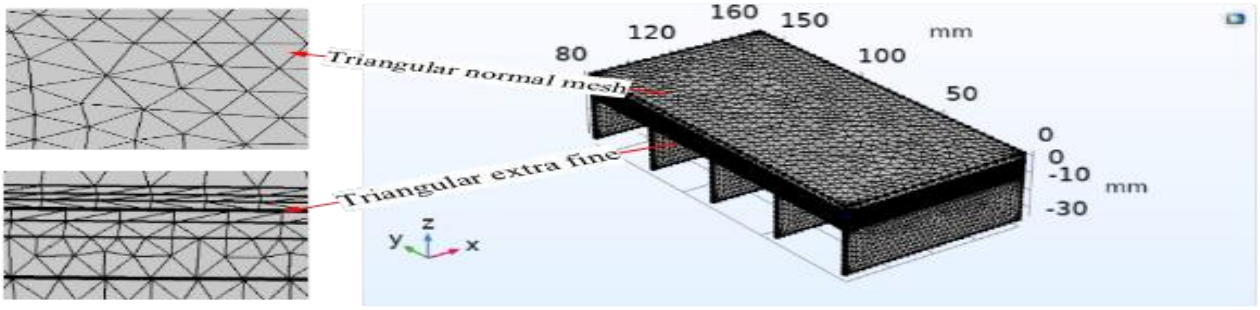

Figure 3. Mesh of the PMD system.

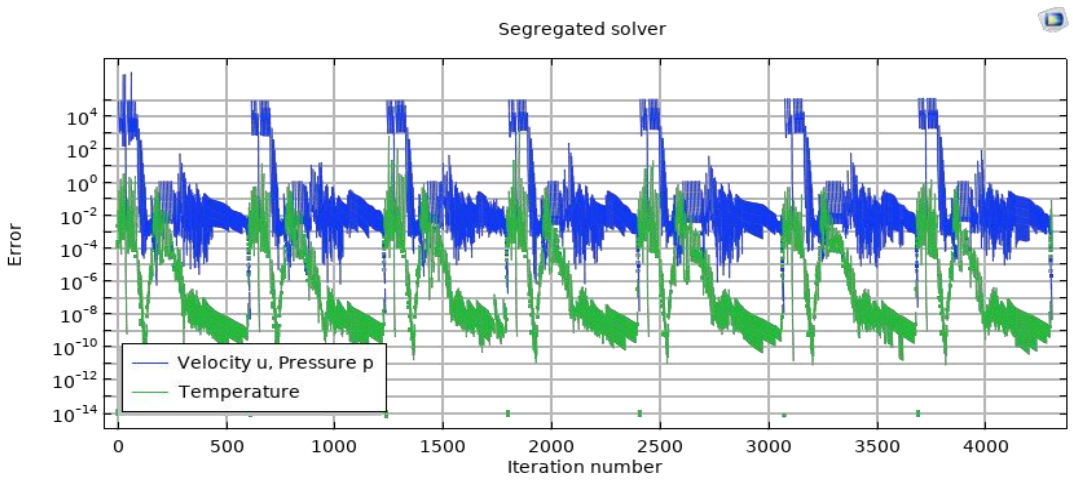

Figure 4. Residuals for the converged numerical solution.

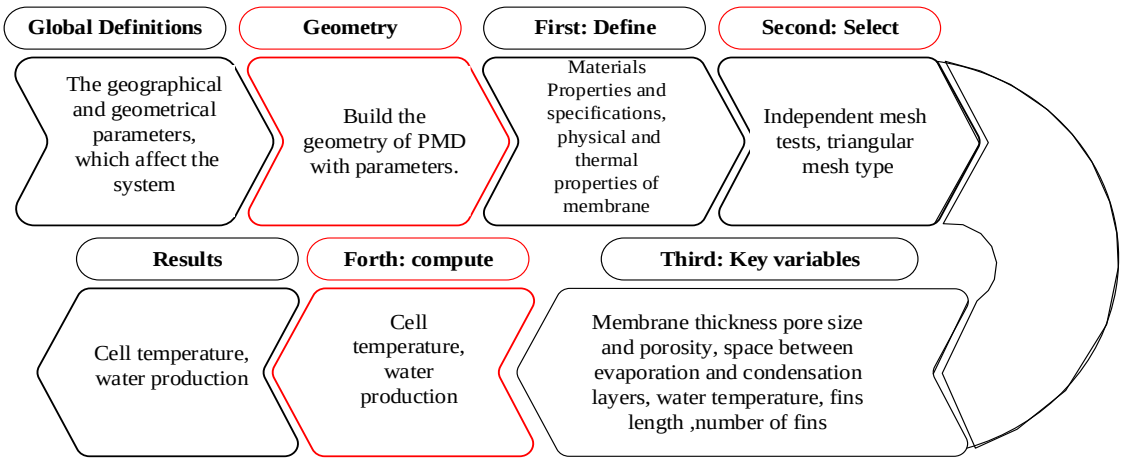

Figure 5. Structure of the COMSOL computation processes in detail.

3.1 Materials Properties and Specifications

The input physical characteristics of materials used in the PMD model were specified using the COMSOL database, and all the properties are listed in Table 2 as follows:

1. The solar panel consisted of five layers: a glass covering, two layers of ethylene-vinyl acetate (EVA), silicon, and a back sheet layer (Tedlar). The input properties were; thermal conductivity (k), coefficient of thermal expansion (α_{iso}) and specific heat (c_p).
2. Water was used for both evaporation layer and condensation layer. The input properties were water density (ρ), water-specific heat (cp) and thermal conductivity (k). All the properties temperature dependent. This layer is consisted of fluid and matrix properties and porous medium permeability(δ). The porosity of mesh is 80%, and the pore size was 25µm.
3. Polytetrafluoroethylene (PTFE) was used as a membrane material. The pore size was 0.45 µm, and the porosity was about of 85%. The input properties were; density(ρ), specific heat (cp) and thermal conductivity (k).
4. Aluminum was used as a conductive and heat sinks material. The input properties were; specific heat (c_p) and thermal conductivity (k).

3.2 Assumptions

The following assumptions were considered in the formulation of the present PMD simulation model:

1. Incompressible and laminar fluid flow through membrane channels.
2. Unsteady state condition with three-dimensional heat transfer for the computational domain.
3. Thermo-physical properties of the fluid were considered as a temperature-dependent.
4. The physical characteristics of the PTFE membrane, density, viscosity, heat capacity and thermal conductivity, were assumed as constant values.
5. The vapor phase was considered as an ideal gas, while the liquid phase was an ideal solution.
6. The temperature of the ambient and solar radiation was time-dependent.
7. The PMD system was perfectly insulated, and the energy loss was neglected negligible.

Table 2.[12] *Thermophysical properties of PV panel and PMD layers.*

No	Material	Thermal conductivity (W/m K)	Density (kg/m^3)	Specific heat (J/kg.K)	Specific heat (J/kg.K)
1	Water	0.625	991	4172	4172
2	PTFE	0.24	2200	1050	1050
3	Silicon	148	2330	677	677
4	EVA	0.35	960	2090	2090
5	Glass	1.8	3000	500	500
6	Tedlar	0.2	1200	1250	1250
7	Aluminum	238	2700	900	900

3.3 Governing Equations

The conservation equations of mass, momentum and energy were the basis of the governing equations used to determine velocity, pressure and temperature distributions in the computational domain of the PMD simulation model. The equations can be written as follows [13], [14],[15]:

I- Conservation equations for non-permeable layers in the PMD system (PV solar panel, Aluminum plate, fins) can be expressed by continuity equations as follows:

$$\frac{\partial \rho}{\partial t}+\rho\left(\frac{\partial u}{\partial x}+\frac{\partial v}{\partial y}+\frac{\partial w}{\partial z}\right)=0 \quad (1)$$

Momentum equation:

$$\rho\frac{\partial u}{\partial t}+\rho(u\frac{\partial u}{\partial x}+u\frac{\partial v}{\partial y}+u\frac{\partial w}{\partial z})=\mu(\frac{\partial^2 u}{\partial x^2}+\frac{\partial^2 u}{\partial y^2}+\frac{\partial^2 u}{\partial z^2})+\rho g-\frac{\partial P}{\partial x} \quad (2)$$

$$\rho\frac{\partial v}{\partial t}+\rho(v\frac{\partial u}{\partial x}+v\frac{\partial v}{\partial y}+v\frac{\partial w}{\partial z})=\mu(\frac{\partial^2 v}{\partial x^2}+\frac{\partial^2 v}{\partial y^2}+\frac{\partial^2 v}{\partial z^2})+\rho g-\frac{\partial P}{\partial y} \quad (3)$$

$$\rho\frac{\partial w}{\partial t}+\rho(w\frac{\partial u}{\partial x}+w\frac{\partial v}{\partial y}+w\frac{\partial w}{\partial z})=\mu(\frac{\partial^2 w}{\partial x^2}+\frac{\partial^2 w}{\partial y^2}+\frac{\partial^2 w}{\partial z^2})+\rho g-\frac{\partial P}{\partial z} \quad (4)$$

Energy equation:

For fluid flow and solar PV pa0nels, the energy equations are:

$$\rho\, C_{\mathrm{p}}\,\frac{\partial T}{\partial t}+\rho\, C_{\mathrm{p}}\left(u\,\frac{\partial T}{\partial x}+v\,\frac{\partial T}{\partial y}+w\,\frac{\partial T}{\partial z}\right)=k\,\left(\frac{\partial^2 T}{\partial x^2}+\frac{\partial^2 T}{\partial y^2}+\frac{\partial^2 T}{\partial z^2}\right)+Q_{in} \quad (5)$$

$$\rho\, C_p\frac{\partial T}{\partial t}=\mathrm{k}\left(\frac{\partial^2 T}{\partial x^2}+\frac{\partial^2 T}{\partial y^2}+\frac{\partial^2 T}{\partial z^2}\right) \quad (6)$$

II- Conservation equations for permeable layers in the *PMD* system (membrane and micro-channels) of the PMD system can be expressed by continuity equation [15]:

$$\frac{1}{\epsilon}\frac{\partial \rho}{\partial t}+\rho\left(\frac{\partial u}{\partial x}+\frac{\partial v}{\partial y}+\frac{\partial w}{\partial z}\right)=0 \quad (7)$$

Momentum equation:

$$\frac{1}{\epsilon}\rho\frac{\partial u}{\partial t}+\frac{1}{\epsilon^2}\rho\left(u\frac{\partial u}{\partial x}+v\frac{\partial u}{\partial y}+w\frac{\partial u}{\partial z}\right)=-\frac{\partial p}{\partial x}+\frac{\mu}{\epsilon}+\frac{\partial^2 u}{\partial x^2}+\frac{\partial^2 u}{\partial y^2}+\frac{\partial^2 u}{\partial z^2}$$
$$-\frac{\mu}{K}u-\frac{\rho_f C_f}{\sqrt{K}}|u|u \quad (8)$$

$$\frac{1}{\epsilon}\rho\frac{\partial v}{\partial t}+\frac{1}{\epsilon^2}\rho\left(u\frac{\partial v}{\partial x}+v\frac{\partial v}{\partial y}+w\frac{\partial v}{\partial z}\right)=-\frac{\partial p}{\partial y}+\frac{\mu}{\epsilon}\left(\frac{\partial^2 v}{\partial x^2}+\frac{\partial^2 v}{\partial y^2}+\frac{\partial^2 v}{\partial z^2}\right)-\frac{\mu}{K}v-$$
$$\frac{\rho_f Cf}{\sqrt{K}}|v|v \quad (9)$$

$$\frac{1}{\epsilon}\rho\frac{\partial w}{\partial t}+\frac{1}{\epsilon^2}\rho\left(u\frac{\partial w}{\partial x}+v\frac{\partial w}{\partial y}+w\frac{\partial w}{\partial z}\right)=-\frac{\partial p}{\partial z}+\frac{\mu}{\epsilon}\left(\frac{\partial^2 w}{\partial x^2}+\frac{\partial^2 w}{\partial y^2}+\frac{\partial^2 w}{\partial z^2}\right)-$$
$$\frac{\mu}{K}w-\frac{\rho_f Cf}{\sqrt{K}}|w|w \quad (10)$$

Energy equation:

$$c_p\epsilon\frac{\partial T}{\partial t}+\rho\, c_p\left(u\frac{\partial T}{\partial x}+v\frac{\partial T}{\partial y}+w\frac{\partial T}{\partial z}\right)=k_{f,eff}\left(\frac{\partial^2 T}{\partial x^2}+\frac{\partial^2 T}{\partial y^2}+\frac{\partial^2 T}{\partial z^2}\right)$$
$$+h_{sf}\, a_{\mathrm{sf}}\,(T_s-T_f) \quad (11)$$

3.4 Calculation of The Production Rate of Clean Water:

According to the membrane distillation theory, the clean water production rate (or vapor flux) that passes through the porous hydrophobic membrane depends on the membrane coefficient and the difference of vapor pressure between the evaporation and condensation layers. The following formula is used to calculate the rate of production:

$$J = \Delta p * c_m \quad (12)$$

The Antoine equation is used to determine the relationship between temperature and vapor pressure (P) in the condensation and evaporation layers [15]:

$$P = \exp\left(A-\frac{B}{C+T}\right) \quad (13)$$

Where A, B, and C for water are constants of values 23.238, 3841, and -45, respectively [15]. Vapor pressure is denoted by P (bar), and temperature by T (K).

The following equation may be used to compute the membrane coefficient(c_m) [16]:

$$c_{\mathrm{m}}=\frac{1}{\frac{3}{2}*\frac{\omega*\delta}{\epsilon*\mathrm{r}}*\left(\frac{\pi*R_o*T}{8\mathrm{M}}\right)^{0.5}+\frac{\tau*\delta}{\epsilon}*\frac{\mathrm{p_a}}{\mathrm{p.D}}*\frac{R*T}{\mathrm{M}}} \quad (14)$$

Where: M= molecular weight of the water (18.02 $\frac{kg}{mol}$), R_o= is the gas constant, $R_o = 8.314\ \frac{\mathrm{kJ}}{\mathrm{mol\,K}}$ and r is pour size of membrane**.**

The following equation may be used to compute the water-air PD and pore tortuosity [17]:

$$\mathrm{P.D} = 1.895*10^{-5}*T^{2.072} \quad (15)$$

$$\omega=\text{pore tortuosity}=\left(\frac{2-\epsilon}{\epsilon}\right)^2 \quad (16)$$

permeability of porous media is determined by [18]:

$$\delta=8.5*(\epsilon*r^2)^{1.3} \quad (17)$$

4. Operating Parameters and Boundary Conditions

4.1 The Geographical and Geometrical Parameters:

The effect of membrane thickness, the space between the evaporation and condensation layer, the height of the fins, the number of fins, and the inlet water temperature on the cell temperature and water productivity were investigated.

4.2 Boundary Conditions:

Based on the computational domain shown in Figure 6, the boundary conditions for fluid and solid walls were assumed as follows:

Solid surface (Walls): No slip condition on solid walls (u= 0, v= 0, w= 0).No thermal jump on the wall. Adiabatic condition for insulated surfaces (q= 0, or dq= 0).

Membrane: The boundary walls were considered as non-slip conditions, and the sides of the membrane layers were assumed to be thermally insulated. The interfaces between the membrane and the channels were considered coupled interfaces.

Solar pane PV: The PV panel's top surface was subjected to a solar radiation G (W/m^2). Convection and radiation heat transfer occurs at the top surface of the PV panel. Conductive heat transfer occurs through the layers of solar PV panels, with negligible thermal contact resistances between the panel layers.

The aluminum sheet: which was attached to the back surface of the solar PV panel, was assumed to be a heat sink with a perfect contact with the back of the PV panel.

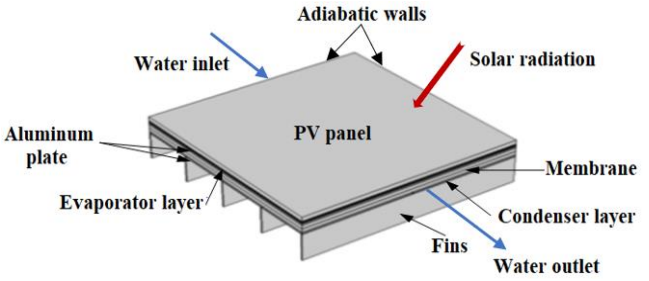

Figure 6. Boundary conditions of the PVM model computational domain.

5. Result and Discussions

It is worth noting that all the cases reviewed have two factors that affect the performance of the cell: the first is cell temperature, and the second is cell water productivity. Although the two factors are essential, the cell temperature is considered to be the critical factor. Value of mass flow rate of the supply water was assumed to be equal to 0.856 kg/h.m^2 according to Wang et al. [19]. Weather conditions of Baghdad (33.3152° N, 44.3661° E), in which the experiments were conducted, are shown in Figure 7.

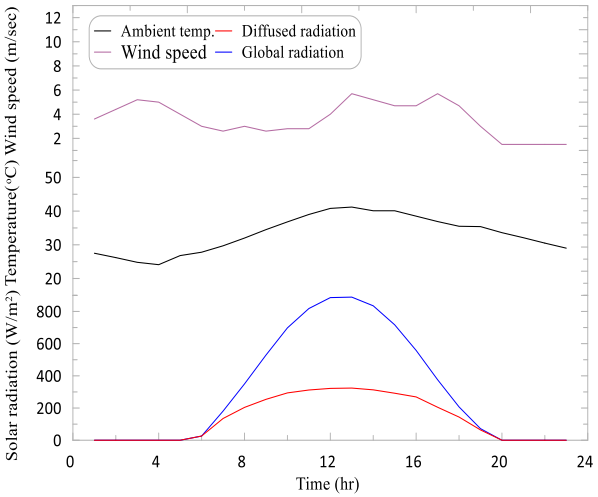

Figure 7. Baghdad Weather conditions.

Validation of the membrane coefficient of the current work with Aleid et al. [3] is shown in Figure 8. The deviation between the two works was about 8%.Moreover, Figure 9 illustrates a comparison between the current theoretical study with Wang et al. [19] the results indicated that the intensity of solar radiation was, approximately, identical for both the studies. However, the difference was observed in the ambient temperature, where, Wang's work exhibited a higher temperature than the current work. This suggests that an increase in cell temperature was observed in the current work. The temperature difference between the cell and the environment was nearly the same in both studies, with an error rate ranging between -1.5 to 4.4%.

The effect of the membrane thickness ranged from 100 to 1000 µm on the temperature polarization for the condensation and evaporation layer is shown in Figure 10. Increasing the membrane thickness increased the temperature of polarization. It clearly observed that the temperature of polarization tended to reduce the difference in the vapor pressure across the membrane.

Figure 11 shows the relation between the membrane thickness and the membrane coefficient (The vapor permeability through the membrane). The results indicated that the thin membrane exhibited a higher membrane coefficient.

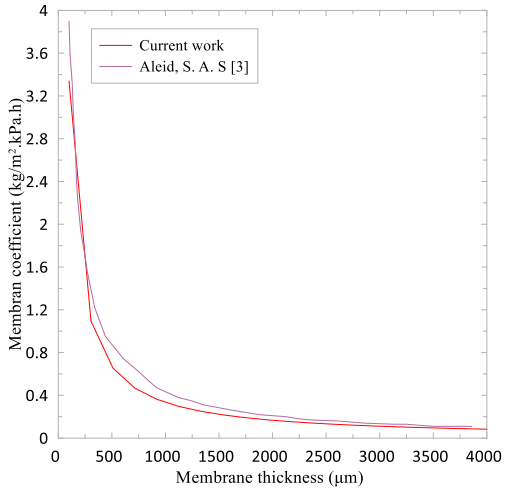

Figure 8. Validation of membrane coefficient.

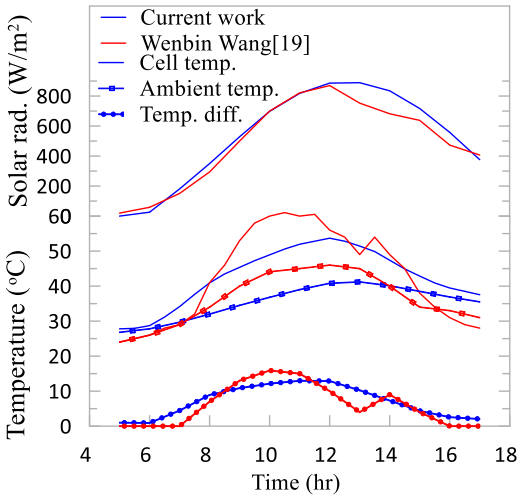

Figure 9. Validation of current work with experiment work.

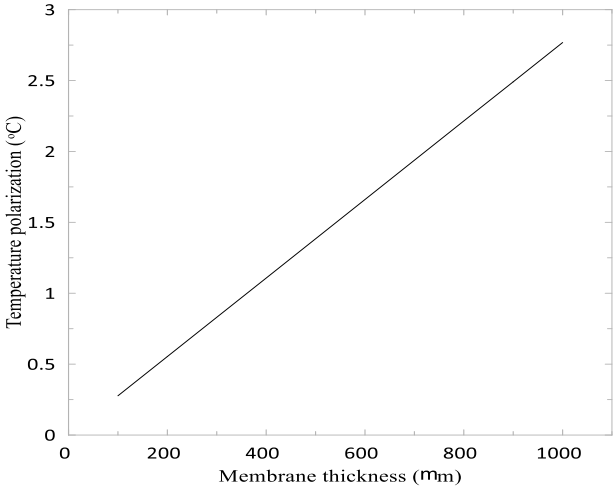

Figure 10. Effect of membrane thickness on the temperature polarization (°C).

Space thickness between the evaporation and condensation layers is a critical factor for providing the temperature difference between evaporation and condensation layers. This temperature difference creates a pressure difference that drives water vapor movement evaporation to condensation layers. This distance can be carried out using two ways: by placing hydrophobic

membranes between them or by placing a mesh [7]. The two methods are adopted to ensure space between the condenser and the evaporator layers. Figures 12 and 13 show the effect of space thickness on the evaporation and condensation temperature. The figures show that the space thickness affects the evaporation temperature more than the condensing temperature. However, the 2.5- and 3-mm space thicknesses show higher evaporation temperatures. The same trends in the first half of the day are observed for the two space thicknesses mentioned. From an economic perspective, the space thickness of 2.5 mm was adopted in the current work.Figure 14 shows the difference between evaporation and condensing temperature for 2.5 mm space thickness. There is no difference between the evaporation and condensing temperatures at night. In daylight time, the difference between the two temperatures rises and reaches a maximum value at noon. Figure 15 shows the effect of the integration of PMD and the PV panel on the cell surface temperature at a space thickness of 2.5 mm. The maximum difference between the cooled and uncooled cell temperatures was about of 7°C at solar noon. The reduction in cell temperature was due to the absorption of cell-stored heat by the water supply.

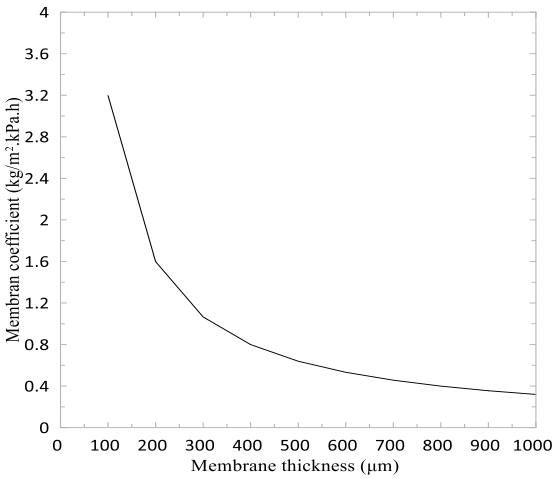

Figure 11. Relation between the membrane thickness and membrane coefficient.

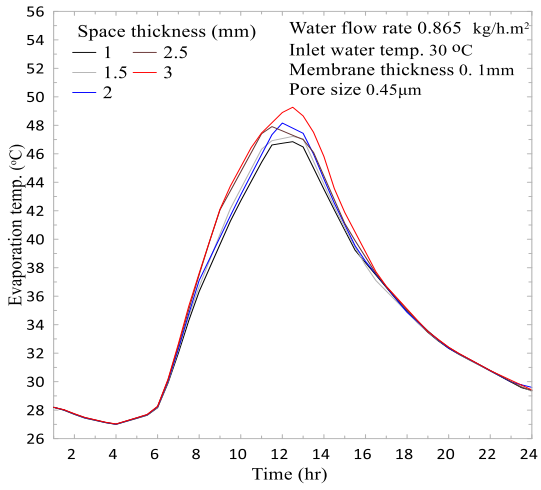

Figure 12. Effect of space thickness on the evaporation temperature.

A heat sink with a base thickness of 1 mm and five fins was attached to the last aluminum layer. The effect of fin height on the cell temperature is shown in Figure 16; the cell's temperature decreases with the increase in the fin's height due to the long fin's ability to dissipate heat more efficiently than the short fin. On the other hand, Figure 17 shows that increasing in the height of the fin reduced the water productivity due to the decrease in cell temperature. So, a trade-off should be made between the two cases. A fin height of 20 mm was chosen to achieve a lower cell temperature and more water productivity.

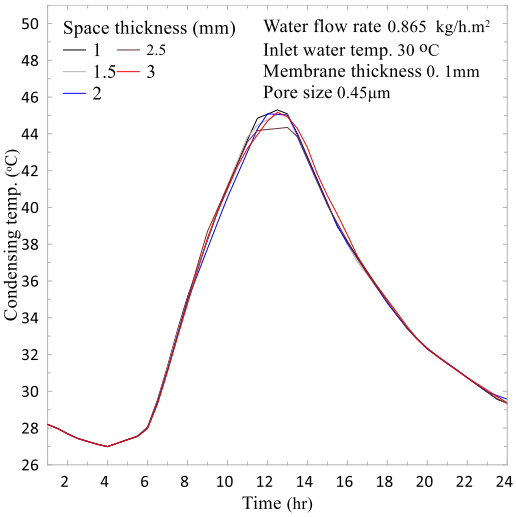

Figure 13. Effect of space thickness on the condensing temperature.

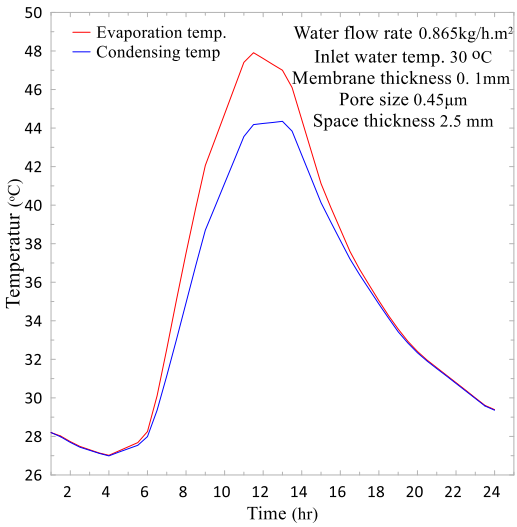

Figure 14. Difference between evaporation and condensing temperature at 2.5 mm space thickness.

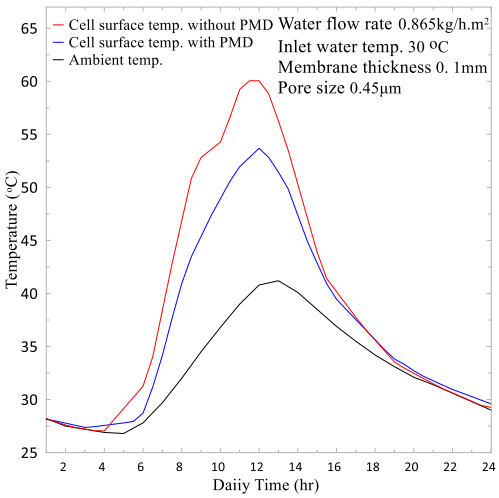

Figure 15. Effect of PMD on the cell surface temperature.

The increasing number of fins reduces the cell temperature, as shown in Figure 18. On the other hand, the water productivity decreases as the number of fins increases according to Figure 19. So, five fins were recommended for the economic point of view and the water productivity. The inlet temperature of the supply water, significantly, affects the cell surface temperature and water productivity, as shown in Figures 20 and 21. Figure 20 indicates that the cell surface temperature decreases as the inlet water temperature decreases. Figure 21 indicates that the low water temperature reduces the water productivity. In any case, the water temperature factor is difficult to control, as the water temperature depends on surrounding weather conditions.

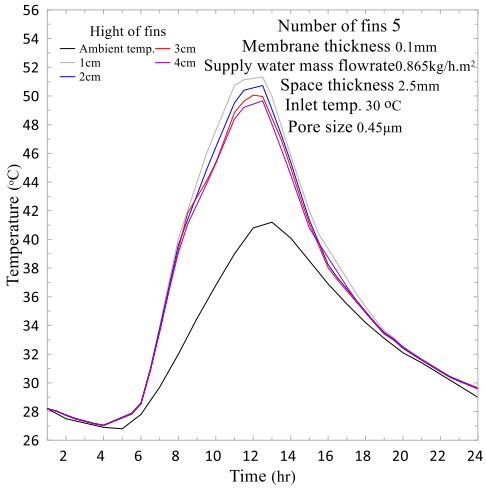

Figure 16. Effect of fin height on the cell temperature.

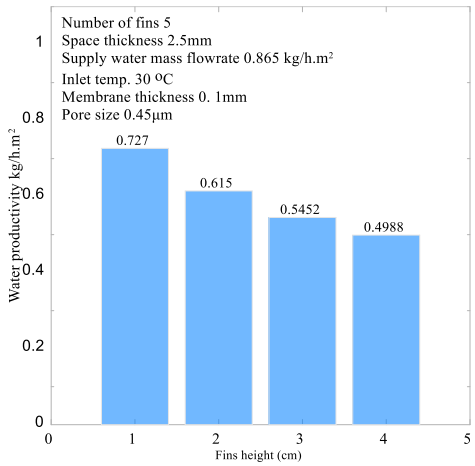

Figure 17. Effect of fin height on water productivity.

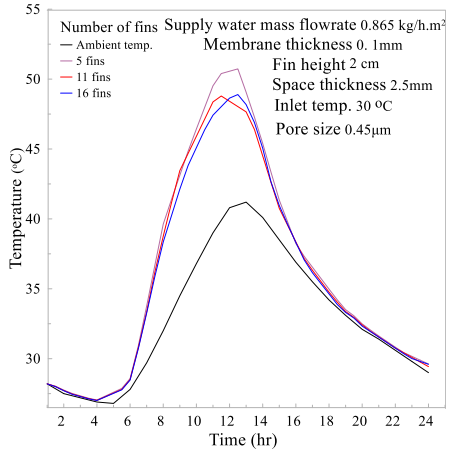

Figure 18. Effect of the number of fins on the cell surface temperature, fins height 20 mm.

Figure 22 shows the final parameter when the water temperature of inlet reached 30 °C, the space between evaporation and condensation was about of 2.5 mm, number of fins was 5 and the height of fins was 20mm in the 3-D plot for temperature distribution on the PMD.

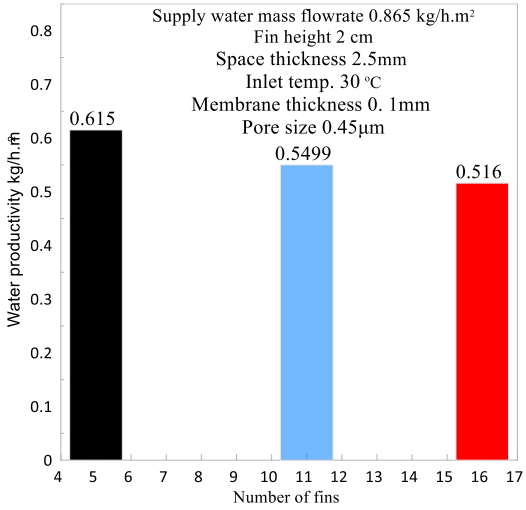

Figure 19. Effect of the number of fins on the water productivity, fins height 2 cm.

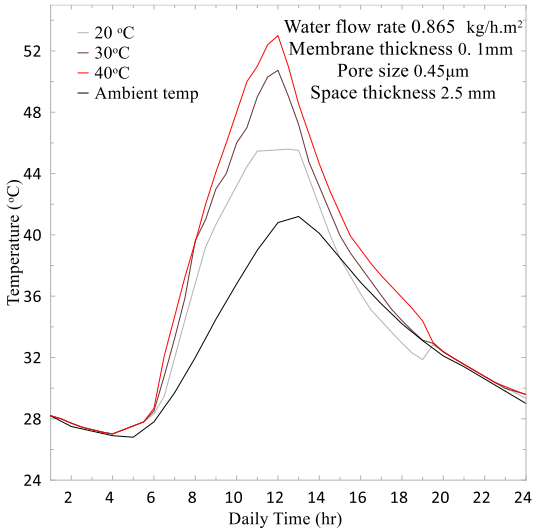

Figure 20. Effect of inlet water temperature on the cell surface temperature.

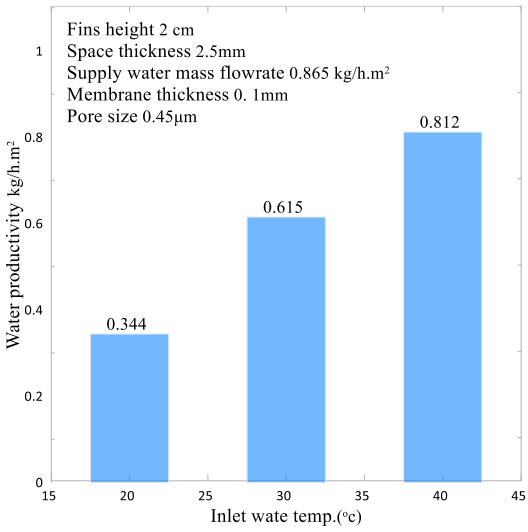

Figure 21. Effect of inlet water temperature on water productivity.

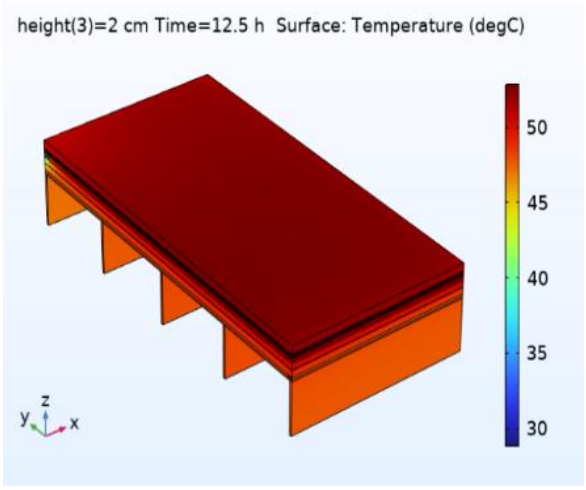

Figure 22. 3-D plot for Temperature distribution on the PMD.

6. Conclusion

From current study, the main conclusions can be drawn as follows:

1. Adding the PMD system to the solar panel reduced the cell surface temperature by 7°C and produced a 0.727 kg/h.m^2 of freshwater.
2. The best membrane thickness was 100 µm, which gave the minimum temperature polarization and the maximum membrane coefficient.
3. The best space between the evaporation and condensation layer was 2.5 mm, which gave a temperature difference of 4°C between the evaporation and condensation layers.
4. Adding a heat sink of five fins with a fin height of 2 cm kept the maximum cell temperature at 50 and yielded water at about of 0.615 kg/h.m^2.

7.Nomenclature

c_p	Specific heat capacity (J/kg. K)	t	Time (sec)
c_m	membrane coefficient ($\frac{kg}{m^2 h\ Pa}$)	Δp	The pressure difference (bar)
J	vapor flux (kg/m^{2}h)	u	Velocity in x-direction (m/sec)
dx	Elements in x_direction (m)	v	Velocity in y-direction (m/sec)
dy	Elements in y_direction (m)	w	Velocity in z-direction (m/sec)
dz	Elements in z_direction (m)		Greek Symbol
g	Gravity (m/sec^2)		
K_f	Thermalconductivity (W/m. K)	ϵ	Porosity of membrane
h	Heat transfer coffeient (W/m^{2}K)	ε	Pore size
pa	Pressure (bar)	µ	Dynamic viscosity (Pa.sec)
Q	Heat source (W/m^2)	ρ	Density (kg/m^3)
T	Temperature (k)	ω	pore tortuosity

References

[1] A. C. Lemay, S. Wagner, and B. P. Rand, "Current status and future potential of rooftop solar adoption in the United States," *Energy Policy*, vol. 177, pp. 113571, Jun. 2023, doi: 10.1016/J.ENPOL.2023.113571.

[2] M. Rabie, M. F. Elkady, and A. H. El-Shazly, "Hybrid membrane distillation/high concentrator photovoltaic system for freshwater production," *Energy Reports*, vol. 8, pp. 112–119, 2022, doi: 10.1016/j.egyr.2021.11.067.

[3] S. Aleid, "Design and Fabrication of Multi-functional Photovoltaic-Membrane Distillation Evaporative Crystallizer for Water Desalination, Electricity Generation, Salt Crystallization and Solar Cell Cooling " M.S. thesis, Dept. Sci. and Tech., Abdullah Univ., Thuwal, Kingdom of Saudi Arabia,2019.

[4] W.Wang, Y.Shi, C.Zhang, S.Hong, L. Shi, J. Chang, R. Li, Y.Jin, C. Ong, S. Zhuo, and P. Wang, "Simultaneous production of fresh water and electricity via multistage solar photovoltaic membrane distillation," *Nat. Commun.*, vol. 10, pp. 3012, Jul. 2019, doi: 10.1038/s41467-019-10817-6.

[5] Q. Zhao, H. Zhang, Z. Hu, and S. Hou, "A solar driven hybrid photovoltaic module/direct contact membrane distillation system for electricity generation and water desalination," *Energy Convers. Manag.*, vol. 221, pp. 113146,Oct.2020,doi:10.1016/j.enconman.2020.113146.

[6] U. Kumar, "Integration of Membrane Distillation and Solar Thermal Systems for Co-production of Purified Water and Heat" Ph.D. dissertation, Dept. Eng. Tech., KTH School of Industrial Engineering and Management., English, 2017.

[7] E. Chiavazzo, M. Morciano, F. Viglino, M. Fasano, and P. Asinari, "Passive solar high-yield seawater desalination by modular and low-cost distillation," *Nat. Sustain.*, vol. 1, no. 12, pp. 763–772, Dec. 2018, doi: 10.1038/s41893-018-0186-x.

[8] A. A. B. Baloch, H. M. S. Bahaidarah, P. Gandhidasan, and F. A. Al-Sulaiman, "Experimental and numerical performance analysis of a converging channel heat exchanger for PV cooling," *Energy Convers. Manag.*, vol. 103, pp. 14–27, Oct. 2015, doi: 10.1016/j.enconman.2015.06.018.

[9] C. G. Popovici, S. V. Hudişteanu, T. D. Mateescu, and N. C. Cherecheş, "Efficiency Improvement of Photovoltaic Panels by Using Air Cooled Heat Sinks," *Energy Procedia*, vol. 85, pp. 425–432, Jan. 2016, doi: 10.1016/j.egypro.2015.12.223.

[10] G. Li and L. Lu, "Modeling and performance analysis of a fully solar-powered stand-alone sweeping gas membrane distillation desalination system for island and coastal households," *Energy Convers. Manag.*, vol. 205, pp. 112375, Feb. 2020, doi: 10.1016/j.enconman.2019.112375.

[11] W. Wang, "The Design and Fabrication of the Multistage-Membrane Distillation Device Integrated with Solar Cell for Simultaneous Water and Electricity Production via Sunlight Dissertation" Ph.D. dissertation, Dept Sci. and Tech., Abdullah Univ., Thuwal, Kingdom of Saudi Arabia,2020.

[12] W. Z. Leow, Y. M. Irwan, I. Safwati, M. Irwanto, A. R. Amelia, Z. Syafiqah, M. I. Fahmi and N. Rosle, "Simulation study on photovoltaic panel temperature under different solar radiation using computational fluid

dynamic method," *J. Phys. Conf. Ser. 1432 012052, Malaysia*, Jan. 2020, vol. 1432, pp. 012052, doi: 10.1088/1742-6596/1432/1/012052.

[13] J. M. Smith, *Introduction to chemical engineering thermodynamics*,6nd Ed.New York: McGraw-Hill,1950.

[14] T. L. Bergman, A. S. Lavine, F. P. Incropera, and D. P. DeWitt, "Fundamental of Heat and Mass Transfer," in *Fluid Mech. its Appl.*,8nd ed. New York: McGraw-Hill, 2011, pp. 321–338. [Online]. Available: https://www.wiley.com/en-us/Fundamentals+of+Heat+and+Mass+Transfer%2C+8th+Edition-p-9781119353881,(Accessed Mar. 04, 2023).

[15] M.D.Koretsky, *Engineering and Chemical Thermodynamics*, 2nd Ed.New York: Wiley, 2012.

[16] A. O. Imdakm and T. Matsuura, "A Monte Carlo simulation model for membrane distillation processes: Direct contact (MD)," *J. Memb. Sci.*, vol. 237, pp. 51–59, Jul. 2004, doi:10.1016/j.memsci.2004.03.005.

[17] S. Srisurichan, R. Jiraratananon, and A. G. Fane, "Mass transfer mechanisms and transport resistances in direct contact membrane distillation process," *J. Memb. Sci.*, vol. 277, pp.186–194, Jun.2006, doi: 10.1016/j.memsci.2005.10.028.

[18] N. Nishiyama and T. Yokoyama, "Permeability of porous media: Role of the critical pore size," *J. Geophys. Res. Solid Earth*, vol. 122,pp. 6955–6971, Aug.2017, doi: 10.1002/2016JB013793.

[19] W. Wang, S. Aleid, Y. Shi, C. Zhang, R. Li, M. Wu, S. Zhu, and P.Wang "Integrated solar-driven PV cooling and seawater desalination with zero liquid discharge," *Joule*, vol. 5, pp. 1873–1887, Jul. 2021, doi: 10.1016/j.joule.2021.05.010.